EUROPEAN ORGANIZATION FOR NUCLEAR RESEARCH

CERN-PH-EP/2006-041
December 13, 2006

Study of Resonance Formation in the Mass Region 1400 – 1500 MeV through the Reaction $\gamma\gamma \to K^0_S K^{\pm}\pi^{\mp}$

L3 Collaboration

Abstract

The $K^0_S K^{\pm}\pi^{\mp}$ final state in two-photon collisions is studied with the L3 detector at LEP at e^+e^- centre-of-mass energies from 183 to 209 GeV with an integrated luminosity of 664.6 pb^{-1}. The $\eta\,(1475)$ and $f_1(1420)$ mesons are observed and their contribution is separated by measuring the formation rates as a function of the photon virtuality Q^2. The $\eta\,(1475)$ is found to be dominant for $Q^2 \leq 0.01$ GeV^2 and its two-photon width is measured to be 0.23 ± 0.05 (stat.)±0.05 (sys.) keV. At higher Q^2, the $f_1(1420)$ is formed and decays to $K^*(892)K$. The $\gamma\gamma$ coupling and form factor parameters of this state are measured to be $\Gamma_{\gamma\gamma} = 3.2 \pm 0.6$ (stat.) $\pm\, 0.7$ (sys.) keV and $\Lambda_1 = 926 \pm 72$ (stat.) $\pm\, 32$ (sys.) MeV, respectively.

Submitted to *Journal of High Energy Physics*

1 Introduction

The study of resonance formation by two virtual photons is well suited to classify $q\bar{q}$ states into SU(3) nonets. Only $C = +1$ resonances can be formed and their two-photon width can be calculated in the framework of quark models. As direct gluon-photon coupling is forbidden, gluonium states are suppressed and the absence of a well-established resonance in the two-photon mass spectrum may be a signature of a gluon-rich partonic structure.

This Letter presents a study of resonance formation by two virtual photons in the reaction $e^+e^- \to e^+e^-\gamma\gamma \to e^+e^-K^0_S K^\pm\pi^\mp$. Untagged two-photon collisions are considered, corresponding to cases where the outgoing electron and positron carry almost the full beam energy and are not detected. The data used for this analysis were collected with the L3 detector [1] at LEP at e^+e^-centre-of-mass energies, $\sqrt{s}$, between 183 GeV and 209 GeV, comprising a total integrated luminosity of 664.6 pb^{-1}.

In the mass region $1400 - 1500$ MeV, two pseudoscalar mesons ($J^{PC} = 0^{-+}$), $\eta\,(1405)$ and $\eta\,(1475)$, and an axial vector meson ($J^{PC} = 1^{++}$), $f_1(1420)$, are observed in the $K^0_S K^\pm\pi^\mp$ final state [2]. The $\eta\,(1405)$, observed in $J/\psi(1S)$ radiative decay and $p\bar{p}$ collisions at rest, also decays into $\eta\pi\pi$ while the $\eta\,(1475)$ decays predominantly to $K\bar{K}\pi$. In a previous Letter [3] we reported the observation of the pseudoscalar $\eta\,(1475)$ and of the axial vector $f_1(1420)$ in the $K^0_S K^\pm\pi^\mp$ final state, but no evidence was found for the $\eta\,(1405)$ either in the $K^0_S K^\pm\pi^\mp$ or in the $\eta\pi^+\pi^-$ final state. The $\eta\,(1475)$ can be identified as the first radial excitation of the η' [4, 5], while the $\eta\,(1405)$ could be a gluonium candidate. The axial vector $f_1(1420)$ was previously observed in two-photon collisions in the $K\bar{K}\pi$ final state by several experiments [6–9]. A recent search for $\eta\,(1475) \to K^0_S K^\pm\pi^\mp$ by the CLEO Collaboration in untagged two-photon events gave a negative result [10]. The same study observed the production of the axial vectors $f_1(1285)$ and $f_1(1420)$ in tagged two-photon collisions [10].

This Letter presents an analysis of the $K^0_S K^\pm\pi^\mp$ final state with the entire L3 statistics obtained during the high-energy LEP runs. This statistics is 50% higher than that used previously [3]. In order to separate the $f_1(1420)$ from the $\eta\,(1475)$, the formation of the resonances is studied as a function of the transverse momentum squared of the $K^0_S K^\pm\pi^\mp$ system, P_T^2. To a good approximation, $P_T^2 = Q^2$, where Q^2 is the largest virtuality of the two interacting photons. Production of spin-one resonances is forbidden for real photons, according to the Landau-Yang theorem [11]. Therefore, at low Q^2, states with spin $J \neq 1$ dominate. The cross section for a resonance R of mass M, spin J, parity P, charge conjugation C and width Γ is:

$$\sigma_{\gamma\gamma\to R} = 8\pi(2J+1)\frac{\Gamma_{\gamma\gamma}\Gamma}{(W^2-M^2)^2+\Gamma^2M^2}F^2_{J^{PC}}(Q^2)\,, \tag{1}$$

where W is the two-photon mass, $\Gamma_{\gamma\gamma}$, the two-photon width, and $F^2_{J^{PC}}(Q^2)$ the square of the form factor. For a spin-one resonance, f_1, the $\gamma\gamma$-coupling parameter is defined [2] as

$$\Gamma_{\gamma\gamma}(f_1) = \lim_{Q^2\to 0}\frac{M^2}{Q^2}\Gamma^{\rm TS}_{\gamma\gamma^*}\,,$$

with $\Gamma^{\rm TS}_{\gamma\gamma^*}$ the partial width for the transverse-scalar two-photon interaction.

In the following, the model of Reference 12 is used. It is based on a hard-scattering approach [13] and describes the Q^2 dependence of the form factors as:

$$F^2_{0^{-+}}(Q^2) = \frac{1}{(1+Q^2/\Lambda_0^2)^2} \tag{2}$$

and

$$F^2_{1^{++}}(Q^2) = \frac{Q^2}{M^2}\Big(1+\frac{Q^2}{2M^2}\Big)\frac{2}{(1+Q^2/\Lambda_1^2)^4} \ , \tag{3}$$

where Λ_0 and Λ_1 are pseudoscalar and axial-vector meson form-factor parameters, respectively. The values of Λ_0 and Λ_1 are expected to be equal to the rho mass, m_ρ, for light mesons and to be closer to the resonance mass for heavier states [12]. The different behaviour of the two form factors as a function of Q^2 is presented in Figure 1.

The same model was used for the analysis of the $f_1(1285) \to \eta\,\pi^+\pi^-$ final state and found to reproduce well the Q^2-dependence of resonance formation [14]. In contrast, the model proposed in Reference 15 and used in previous analyses [6, 7] with a form factor

$$F^2_{1^{++}}(Q^2) = \frac{Q^2}{M^2}\Big(1+\frac{Q^2}{2M^2}\Big)\frac{2}{(1+Q^2/m_\rho^2)^2} \tag{4}$$

was excluded by the data [14].

2 Monte Carlo Generators

Two Monte Carlo generators are used in this study to describe two-photon resonance formation: EGPC [16] and GaGaRes [17].

The EGPC Monte Carlo describes the two-photon process as the product of the luminosity function for transverse photons [18] and the resonance production cross section. It is used to tune event selection criteria and calculate selection efficiencies. The decay distributions of the resonance are generated according to Lorentz invariant phase-space. About 10^5 Monte Carlo events are generated for each of three resonance masses: 1.41 GeV, 1.44 GeV and 1.48 GeV. Only one value of the e^+e^- center-of-mass energy is generated, $\sqrt{s} = 189$ GeV, since detector efficiencies and Q^2 distributions are found to have a very weak dependence on $\sqrt{s}$ for the energy range investigated. The events are passed through the L3 detector simulation based on the GEANT [19] and GEISHA [20] programs. Time-dependent detector efficiencies, as monitored during the data-taking period, are also simulated.

The GaGaRes generator, which calculates a matrix element for the process $e^+e^- \to e^+e^- R$, describes the Q^2 dependence of resonance formation according to the form factors given in formulae (2) and (3). It is used to compare the experimental cross sections with the expectations and to extract the resonance parameters $\Gamma_{\gamma\gamma}(\eta)$, $\Gamma_{\gamma\gamma}(f_1)$, Λ_0 and Λ_1.

3 Event Selection

The events are collected by two charged-track triggers. The first trigger [21] requires at least two wide-angle tracks, back-to-back within $\pm 41^\circ$ in the plane transverse to the beam. The second trigger [22] is based on an artificial neural network which was trained to select low-multiplicity events while rejecting beam-gas and beam-wall background.

The procedure to select $e^+e^- \to e^+e^- K^0_S\, K^\pm\pi^\mp$ events is similar to that used in the previous analysis [3]. Events are selected by requiring four charged particles in the central tracker associated to two vertices: two tracks associated to the e^+e^- interaction point, and a pair of tracks coming from a secondary vertex, corresponding to K^0_S decay into $\pi^+\pi^-$. The tracks must have more than 9 hits and the number of hits must be greater than 60% of that expected from the track length. The secondary vertex must be at least 2 mm away from the e^+e^- interaction

point in the plane transverse to the beam. The mass of the $\pi^+\pi^-$ system, shown in Figure 2a, must be in the range $470 - 520$ MeV.

The $K^\pm$ and $\pi^\mp$ tracks are identified by the dE/dx measurements shown in Figure 2b. For each pair of particles, a joint χ^2 is calculated for the hypotheses $\pi^+\pi^-$, K^+K^- or $K^\pm\pi^\mp$. The identification requires a confidence level (CL) greater than 5% for the hypothesis $K^\pm\pi^\mp$ while the charge-conjugate hypothesis, $K^\mp\pi^\pm$, must have a CL<3%, in order resolve the $K-\pi$ ambiguity. The hypotheses $\pi^+\pi^-$ and K^+K^- must have a CL<10%. Since the 4π background is higher at low Q^2, the confidence level for dE/dx identification for the hypothesis $\pi^+\pi^-$ is lowered to 0.1% for $Q^2 < 0.12$ GeV^2. For $Q^2 > 0.4$ GeV^2, the dE/dx performance degrades, but the background is lower, therefore events are accepted if they satisfy one of the following requirements: the same dE/dx criteria as for the $0.12 < Q^2 < 0.4$ GeV^2 range; all tracks have at least 20 hits; the secondary vertex is at least 4 mm away in the transverse plane from the e^+e^- interaction point.

Events with candidate photons are rejected. An electromagnetic cluster, with energy greater than 100 MeV, is considered as a candidate photon if it is separated from all tracks by more than 0.2 radians. Events with a second K^0_S candidate are also rejected.

This selection results in 820 events with a $K^0_S\,K^\pm\pi^\mp$ effective mass below 2.7 GeV and Q^2 in the range $0 - 7$ GeV^2.

4 Results

4.1 Q^2 Dependence

For the following analysis, the data is subdivided into five Q^2 ranges listed in the first column of Table 1. The corresponding $K^0_S\,K^\pm\pi^\mp$ effective mass spectra for the five Q^2 ranges are presented in Figure 3. A clear peak between 1.35 GeV and 1.55 GeV is present in each sub-sample. At high Q^2-values, another peak, which we associate with the $f_1(1285)$ meson, is also seen.

Each mass spectrum of Figure 3 is fitted with a Gaussian function over a background function of the form $(W-1.16)^2\,\exp(p_1+p_2W^2)$, where W is the $K^0_S\,K^\pm\pi^\mp$ mass and 1.16 GeV is the edge of the mass spectrum. For the spectra above $Q^2 > 0.12$ GeV^2, an additional Gaussian function, representing the $f_1(1285)$, is added with a fixed mass, $M = 1282$ MeV [2], and a fixed width corresponding to the experimental mass resolution, $\sigma = 20$ MeV.

The peak yield for each Q^2-range is presented in Table 1 together with the mass and width obtained by the fit. Table 1 also presents the trigger efficiencies. These are evaluated by using the data themselves comparing the rates of two independent triggers. The selection efficiencies are also listed in the Table. They are determined as the ratio of selected to generated Monte Carlo events in the mass range around the resonance peak. The efficiencies are estimated for each Q^2 interval. The trigger efficiency decreases at higher Q^2 due to the back-to-back requirement imposed on the tracks. In contrast, the geometrical acceptance of the detector increases with increasing Q^2 .

The numbers of events in the peak are compared in Figure 4a to the expectations of the GaGaRes Monte Carlo for the formation of a single pseudoscalar meson, $\eta\,(1475)$, or a single axial-vector meson, $f_1(1420)$. A χ^2 comparison of the five bins of this histogram gives a confidence level of 3×10^{-4} for the $f_1(1420)$ hypothesis and 6×10^{-9} for the $\eta\,(1475)$ hypothesis. Therefore the data cannot be described by a single pseudoscalar or axial-vector meson: both states must be included in a fit to the mass spectra. In addition, there is no evidence that also the formation of $\eta\,(1405)$ or $f_1(1510)$ must be included, consistent with a gluon-rich partonic

structure for these states.

4.2 Global Fit

The five $K^0_S\,K^\pm\pi^\mp$ mass spectra are fitted simultaneously with a binned maximum-likelihood method, using a mass bin of 5 MeV[1)], in the hypothesis of the presence of both pseudoscalar and axial-vector resonances. The relative yield of the resonances as a function of Q^2 is fixed according to the GaGaRes program. Each resonance is described by the convolution of a Breit-Wigner function with a Gaussian resolution function estimated by Monte Carlo. The resolution is of the order of $\sigma = 20$ MeV.

The free parameters of the fit are: the mass of each resonance; the $\eta\,(1475)$ width; the Λ_1 parameter of the $f_1(1420)$ form factor and the overall normalisation of each resonance. The $f_1(1420)$ width is fixed to the world average value, $\Gamma = 55$ MeV [2]. If this parameter is left free the fit becomes unstable. The Λ_0 parameter of the $\eta\,(1475)$ form factor cannot be determined as most of the $\eta\,(1475)$ data is in a single bin. It is fixed to the theoretical value 1470 MeV [12].

As in the previous fit a Q^2-dependent background is used. The parameters p_1 and p_2 of the background are determined separately in each Q^2 interval and the $f_1(1285)$ is added to the background function in the high Q^2 intervals.

The results of the fit are given in Table 2 and presented in Figures 4b and 5. The production cross section is calculated from the number of events, the efficiency and the luminosity. The two-photon width is then extracted by comparing this cross section to that estimated by the GaGaRes program. The correlation coefficients of the parameters of interest are given in Table 3. A χ^2 comparison of this fit to the five bins presented in Figure 4b gives a confidence level of 22%. The total number of events in the $f_1(1285)$ peak is found to be 19.8 ± 4.4. The limited statistics and the uncertainties of the efficiency corrections at threshold prevent further investigation of the formation of this resonance.

4.3 Systematic Uncertainties

Different sources of systematic uncertainties on the $\eta\,(1475)$ and $f_1(1420)$ parameters are considered, as listed in Table 4. They are estimated by varying the selection cuts, the fixed parameters of the fit and taking into account the uncertainties on the total efficiencies:

- The K^0_S mass window, shown by the arrows in Figure 2a, is extended to $465 - 525$ MeV and narrowed to $475 - 515$ MeV.
- The cut on the distance, in the transverse plane, of the K^0_S decay vertex from the interaction point is varied to 3 mm for $Q^2 < 0.4$ GeV^2 and to 4 mm for higher Q^2.
- The $\mathrm{d}E/\mathrm{d}x$ selection cut against a $\pi^+\pi^-$ pair at the primary vertex is varied to CL<1% for $Q^2 < 0.12$ GeV^2, to CL<10% for $0.12 < Q^2 < 0.4$ GeV^2 and completely removed for $Q^2 > 0.4$ GeV^2.
- The form factor parameter of the $\eta\,(1475)$ is varied from the fixed value $\Lambda_0 = 1470$ GeV to $\Lambda_0 = m_\rho$.
- The width of $f_1(1420)$ is varied between 50 MeV and 60 MeV.

[1)] The bin width was varied between 2 MeV and 6 MeV and no significant difference in the results was observed.

4.4 The $\eta\,(1475)$ Resonance

In the first Q^2 bin of Figure 5a, the spin-0 contribution dominates. The mass and width of the peak, $M = 1469 \pm 14$ (stat.)± 13 (sys.) MeV and $\Gamma = 67 \pm 18$ (stat.)± 7 (sys.) MeV, are consistent with the world average values for the $\eta\,(1475)$: $M = 1476 \pm 4$ MeV and $\Gamma = 87 \pm 9$ MeV [2]. The form factor parameter Λ_0 is fixed in the fit to 1470 MeV, near to the resonance mass value. If released, its value is unstable, due to the rapid Q^2-dependence of the pseudoscalar yield. However, a variation of this value down to m_ρ has a small effect on the fit results, as shown in Table 4. The two-photon width of the $\eta\,(1475)$ decay into $\mathrm{K\bar{K}}\pi$ is obtained taking into account the branching ratios $\mathrm{BR}(\mathrm{K^0_S} \to \pi^+\pi^-) = 0.6895$ and the ratio $\mathrm{K^0_S\,K^\pm\pi^\mp/K\bar{K}}\pi = 1/3$ [2]. The value $\Gamma_{\gamma\gamma}(\eta\,(1475))\mathrm{BR}(\mathrm{K\bar{K}}\pi) = 230 \pm 50$ (stat.) ± 50 (sys.) eV, listed in Table 2, is consistent with and supersedes our previous result [3]. This is the only existing measurement, since the recent search by the CLEO Collaboration [10] shows no signal in the $\eta\,(1475)$ region of the $\mathrm{K^0_S\,K^\pm\pi^\mp}$ mass spectrum, with an upper limit $\Gamma_{\gamma\gamma}(\eta\,(1475))\mathrm{BR}(\mathrm{K\bar{K}}\pi) < 89$ eV at 90% CL. However, according to Figure 10 of Reference 10, this upper limit increases to ~ 140 eV if the world average width of the $\eta\,(1475)$ is used, a value which is not inconsistent with the measurement reported in this Letter.

4.5 The $\mathrm{f_1(1420)}$ Resonance

The production of the axial-vector meson $\mathrm{f_1}(1420)$ dominates the mass spectra at high Q^2 values. Its width is fixed to 55 MeV in the fit, in accordance with the world average value $\Gamma = 54.9 \pm 2.6$ MeV [2]. The fitted mass is $M = 1434 \pm 5$ (stat.) ± 5 (sys.) MeV, consistent with the world average value $M = 1426.3 \pm 0.9$ MeV [2] and the CLEO measurement $M = 1441.3 \pm 3$ MeV [10].

The two-photon coupling parameter of the $\mathrm{f_1}(1420)$ is $\Gamma_{\gamma\gamma}(\mathrm{f_1}(1420))\mathrm{BR}(\mathrm{K\bar{K}}\pi) = 3.2 \pm 0.6$ (stat.) ± 0.7 (sys.) keV. A comparison with previous results [6–9] is difficult due to the limited statistics of those data and to the different methods used to extract the two-photon coupling. Our similar analysis of the state $\mathrm{f_1}(1285)$ in the $\eta\,\pi^+\pi^-$ decay mode, gives $\Gamma_{\gamma\gamma}(\mathrm{f_1}(1285)) = 3.5 \pm 0.6$ (stat.) ± 0.5 (sys.) keV [14]. Assigning the $\mathrm{f_1}(1285)$ and $\mathrm{f_1}(1420)$ mesons as the $I = 0$ members of the 1^{++} $\mathrm{q\bar{q}}$ nonet, and assuming that $\mathrm{f_1}(1420)$ decays only into $\mathrm{K\bar{K}}\pi$, the singlet-octet mixing angle θ_A of the axial-vector nonet is determined from [7]:

$$\frac{\Gamma_{\gamma\gamma}(\mathrm{f_1}(1285))}{\Gamma_{\gamma\gamma}(\mathrm{f_1}(1420))} = \frac{M(\mathrm{f_1}(1285))}{M(\mathrm{f_1}(1420))}\ \cot^2(\theta_A - \theta_0)\,, \tag{5}$$

where $\theta_0 = \arcsin(1/3)$. Using the world-average values for the meson masses [2], the L3 measurements result in $\theta_A = 62^\circ \pm 5^\circ$. This value is compatible with other estimations [23].

The form factor parameter is found to be $\Lambda_1 = 926 \pm 72$ (stat.)± 32 (sys.) MeV. This value is similar to the one found for the $\mathrm{f_1}(1285)$ axial vector, $\Lambda_1 = 1040 \pm 60$ (stat.)± 50 (sys.) MeV [14], indicating a similar production mechanism for the two resonances.

4.6 The $\mathrm{f_1(1420) \to K^*(892)K}$ Decay

To search for the decay $\mathrm{f_1}(1420) \to \mathrm{K^*}(892)\mathrm{K}$ in the $\mathrm{K^0_S\,K^\pm\pi^\mp}$ final state, only data with $Q^2 > 0.4$ GeV^2 are selected, where $\mathrm{f_1}(1420)$ production dominates. Two-dimensional distributions of the $\mathrm{K^0_S}\pi^\pm$ and $\mathrm{K^\pm\pi^\mp}$ masses for each event are shown in Figure 6 for all the $\mathrm{K^0_S\,K^\pm\pi^\mp}$ events and for the resonance region only: 1320 MeV $\leq M(\mathrm{K^0_S\,K^\pm\pi^\mp}) \leq$ 1570 MeV. In both plots the data accumulate in bands around the $\mathrm{K^*}(892)$ mass value. Figure 6b, where only $\mathrm{f_1}(1420)$

events are selected, displays these accumulations more distinctly, with a lower background level outside the $K^*(892)$ bands.

The projections on the $M(K^0_S\pi^\pm)$ and $M(K^\pm\pi^\mp)$ axes for the resonance region are presented in Figure 7. The spectra are fitted with a resonance over a background function. The resonance is described by the convolution of a Breit-Wigner of fixed width, $\Gamma(K^*(892)) = 51$ MeV [2], and resolution of 15 MeV for the $K^0_S\pi^\pm$ system and 9 MeV for the $K^\pm\pi^\mp$ system, estimated by Monte Carlo simulations. The background is described by the function $(M(K\pi)-0.6)^2\ \exp(a+bM(K\pi)^2)$, where 0.6 GeV is the edge of the $K\pi$ spectra and a and b are free parameters. Table 5 presents the results of the fit. Each decay channel contains about 65 events in the $K^*(892)$ peak. This result, when compared to the 68 events obtained in the global fit for the $f_1(1420)$ peak, is consistent with the resonance decay entirely through $K^*(892)K$, as previously observed [2].

5 Conclusion

The exclusive $K^0_S\,K^\pm\pi^\mp$ final state is studied in two-photon interactions with the full high energy statistics collected by L3 at LEP. A significant enhancement in the mass spectra is observed in the region $1.35-1.55$ GeV for the Q^2 range $0-7$ GeV^2. The Q^2-dependent mass spectra cannot be described by the formation of a single pseudoscalar or a single axial-vector meson. Contributions of both the $\eta\,(1475)$ and $f_1(1420)$ resonances are required. The $\eta\,(1475)$ signal dominates at $Q^2 < 0.01$ GeV^2 and has a statistical significance of 4.6 standard deviations. The $f_1(1420)$ dominates for $Q^2 > 0.4$ GeV^2 and decays entirely through $K^*(892)K$. The two-photon couplings and the form factors of these resonances are well described by the formalism of Reference 12 with the following parameters:

$$\begin{aligned}
\Gamma_{\gamma\gamma}(\eta\,(1475))\mathrm{BR}(K\bar{K}\pi) = &\quad 230 \pm 50\ (\mathrm{stat.}) \pm 50\ (\mathrm{sys.})\ \ \mathrm{eV},\\
\Gamma_{\gamma\gamma}(f_1(1420))\mathrm{BR}(K\bar{K}\pi) = &\quad 3.2 \pm 0.6\ (\mathrm{stat.}) \pm 0.7\ (\mathrm{sys.})\ \mathrm{keV},\\
\Lambda_1 = &\quad 926 \pm 72\ (\mathrm{stat.}) \pm 32\ (\mathrm{sys.})\ \mathrm{MeV}.
\end{aligned}$$

The production of $f_1(1285)$ is also observed in data, while no signals of the of $\eta\,(1405)$ or $f_1(1510)$ mesons are observed.

Author List

The L3 Collaboration:

P.Achard,[20] O.Adriani,[17] M.Aguilar-Benitez,[25] J.Alcaraz,[25] G.Alemanni,[23] J.Allaby,[18] A.Aloisio,[29] M.G.Alviggi,[29] H.Anderhub,[49] V.P.Andreev,[6,34] F.Anselmo,[8] A.Arefiev,[28] T.Azemoon,[3] T.Aziz,[9] P.Bagnaia,[39] A.Bajo,[25] G.Baksay,[26] L.Baksay,[26] S.V.Baldew,[2] S.Banerjee,[9] Sw.Banerjee,[4] A.Barczyk,[49,47] R.Barillère,[18] P.Bartalini,[23] M.Basile,[8] N.Batalova,[46] R.Battiston,[33] A.Bay,[23] F.Becattini,[17] U.Becker,[13] F.Behner,[49] L.Bellucci,[17] R.Berbeco,[3] J.Berdugo,[25] P.Berges,[13] B.Bertucci,[33] B.L.Betev,[49] M.Biasini,[33] M.Biglietti,[29] A.Biland,[49] J.J.Blaising,[4] S.C.Blyth,[35] G.J.Bobbink,[2] A.Böhm,[1] L.Boldizsar,[12] B.Borgia,[39] S.Bottai,[17] D.Bourilkov,[49] M.Bourquin,[20] S.Braccini,[20] J.G.Branson,[41] F.Brochu,[4] J.D.Burger,[13] W.J.Burger,[33] X.D.Cai,[13] M.Capell,[13] G.Cara Romeo,[8] G.Carlino,[29] A.Cartacci,[17] J.Casaus,[25] F.Cavallari,[39] N.Cavallo,[36] C.Cecchi,[33] M.Cerrada,[25] M.Chamizo,[20] Y.H.Chang,[44] M.Chemarin,[24] A.Chen,[44] G.Chen,[7] G.M.Chen,[7] H.F.Chen,[22] H.S.Chen,[7] G.Chiefari,[29] L.Cifarelli,[40] F.Cindolo,[8] I.Clare,[13] R.Clare,[38] G.Coignet,[4] N.Colino,[25] S.Costantini,[39] B.de la Cruz,[25] S.Cucciarelli,[33] R.de Asmundis,[29] P.Déglon,[20] J.Debreczeni,[12] A.Degré,[4] K.Dehmelt,[26] K.Deiters,[47] D.della Volpe,[29] E.Delmeire,[20] P.Denes,[37] F.DeNotaristefani,[39] A.De Salvo,[49] M.Diemoz,[39] M.Dierckxsens,[2] C.Dionisi,[39] M.Dittmar,[49] A.Doria,[29] M.T.Dova,[10,♯] D.Duchesneau,[4] M.Duda,[1] B.Echenard,[20] A.Eline,[18] A.El Hage,[1] H.El Mamouni,[24] A.Engler,[35] F.J.Eppling,[13] P.Extermann,[20] M.A.Falagan,[25] S.Falciano,[39] A.Favara,[32] J.Fay,[24] O.Fedin,[34] M.Felcini,[49] T.Ferguson,[35] H.Fesefeldt,[1] E.Fiandrini,[33] J.H.Field,[20] F.Filthaut,[31] P.H.Fisher,[13] W.Fisher,[37] G.Forconi,[13] K.Freudenreich,[49] C.Furetta,[27] Yu.Galaktionov,[28,13] S.N.Ganguli,[9] P.Garcia-Abia,[25] M.Gataullin,[32] S.Gentile,[39] S.Giagu,[39] Z.F.Gong,[22] G.Grenier,[24] O.Grimm,[49] M.W.Gruenewald,[16] V.K.Gupta,[37] A.Gurtu,[9] L.J.Gutay,[46] D.Haas,[5] D.Hatzifotiadou,[8] T.Hebbeker,[1] A.Hervé,[18] J.Hirschfelder,[35] H.Hofer,[49] M.Hohlmann,[26] G.Holzner,[49] S.R.Hou,[44] B.N.Jin,[7] P.Jindal,[14] L.W.Jones,[3] P.de Jong,[2] I.Josa-Mutuberría,[25] M.Kaur,[14] M.N.Kienzle-Focacci,[20] J.K.Kim,[43] J.Kirkby,[18] W.Kittel,[31] A.Klimentov,[13,28] A.C.König,[31] M.Kopal,[46] V.Koutsenko,[13,28] M.Kräber,[49] R.W.Kraemer,[35] A.Krüger,[48] A.Kunin,[13] P.Ladron de Guevara,[25] I.Laktineh,[24] G.Landi,[17] M.Lebeau,[18] A.Lebedev,[13] P.Lebrun,[24] P.Lecomte,[49] P.Lecoq,[18] P.Le Coultre,[49] J.M.Le Goff,[18] R.Leiste,[48] M.Levtchenko,[27] P.Levtchenko,[34] C.Li,[22] S.Likhoded,[48] C.H.Lin,[44] W.T.Lin,[44] F.L.Linde,[2] L.Lista,[29] Z.A.Liu,[7] W.Lohmann,[48] E.Longo,[39] Y.S.Lu,[7] C.Luci,[39] L.Luminari,[39] W.Lustermann,[49] W.G.Ma,[22] L.Malgeri,[18] A.Malinin,[28] C.Maña,[25] J.Mans,[37] J.P.Martin,[24] F.Marzano,[39] K.Mazumdar,[9] R.R.McNeil,[6] S.Mele,[18,29] L.Merola,[29] M.Meschini,[17] W.J.Metzger,[31] A.Mihul,[11] H.Milcent,[18] G.Mirabelli,[39] J.Mnich,[1] G.B.Mohanty,[9] G.S.Muanza,[24] A.J.M.Muijs,[2] M.Musy,[39] S.Nagy,[15] S.Natale,[20] M.Napolitano,[29] F.Nessi-Tedaldi,[49] H.Newman,[32] A.Nisati,[39] T.Novak,[31] H.Nowak,[48] R.Ofierzynski,[49] G.Organtini,[39] I.Pal,[46] C.Palomares,[25] P.Paolucci,[29] R.Paramatti,[39] G.Passaleva,[17] S.Patricelli,[29] T.Paul,[10] M.Pauluzzi,[33] C.Paus,[13] F.Pauss,[49] M.Pedace,[39] S.Pensotti,[27] D.Perret-Gallix,[4] D.Piccolo,[29] F.Pierella,[8] M.Pieri,[41] M.Pioppi,[33] P.A.Piroué,[37] E.Pistolesi,[27] V.Plyaskin,[28] M.Pohl,[20] V.Pojidaev,[17] J.Pothier,[18] D.Prokofiev,[34] G.Rahal-Callot,[49] M.A.Rahaman,[9] P.Raics,[15] N.Raja,[9] R.Ramelli,[49] P.G.Rancoita,[27] R.Ranieri,[17] A.Raspereza,[48] P.Razis,[30] S.Rembeczki,[26] D.Ren,[49] M.Rescigno,[39] S.Reucroft,[10] S.Riemann,[48] K.Riles,[3] B.P.Roe,[3] L.Romero,[25] A.Rosca,[48] C.Rosemann,[1] C.Rosenbleck,[1] S.Rosier-Lees,[4] S.Roth,[1] J.A.Rubio,[18] G.Ruggiero,[17] H.Rykaczewski,[49] A.Sakharov,[49] S.Saremi,[6] S.Sarkar,[39] J.Salicio,[18] E.Sanchez,[25] C.Schäfer,[18] V.Schegelsky,[34] H.Schopper,[21] D.J.Schotanus,[31] C.Sciacca,[29] L.Servoli,[33] S.Shevchenko,[32] N.Shivarov,[42] V.Shoutko,[13] E.Shumilov,[28] A.Shvorob,[32] D.Son,[43] C.Souga,[24] P.Spillantini,[17] M.Steuer,[13] D.P.Stickland,[37] B.Stoyanov,[42] A.Straessner,[20] K.Sudhakar,[9] G.Sultanov,[42] L.Z.Sun,[22] S.Sushkov,[1] H.Suter,[49] J.D.Swain,[10] Z.Szillasi,[26,¶] X.W.Tang,[7] P.Tarjan,[15] L.Tauscher,[5] L.Taylor,[10] B.Tellili,[24] D.Teyssier,[24] C.Timmermans,[31] Samuel C.C.Ting,[13] S.M.Ting,[13] S.C.Tonwar,[9] J.Tóth,[12] C.Tully,[37] K.L.Tung,[7] J.Ulbricht,[49] E.Valente,[39] R.T.Van de Walle,[31] R.Vasquez,[46] G.Vesztergombi,[12] I.Vetlitsky,[28] G.Viertel,[49] M.Vivargent,[4] S.Vlachos,[5] I.Vodopianov,[26] H.Vogel,[35] H.Vogt,[48] I.Vorobiev,[35,28] A.A.Vorobyov,[34] M.Wadhwa,[5] Q.Wang,[31] X.L.Wang,[22] Z.M.Wang,[22] M.Weber,[18] S.Wynhoff,[37,†] L.Xia,[32] Z.Z.Xu,[22] J.Yamamoto,[3] B.Z.Yang,[22] C.G.Yang,[7] H.J.Yang,[3] M.Yang,[7] S.C.Yeh,[45] An.Zalite,[34] Yu.Zalite,[34] Z.P.Zhang,[22] J.Zhao,[22] G.Y.Zhu,[7] R.Y.Zhu,[32] H.L.Zhuang,[7] A.Zichichi,[8,18,19] B.Zimmermann,[49] M.Zöller.[1]

1 III. Physikalisches Institut, RWTH, D-52056 Aachen, Germany[§]
2 National Institute for High Energy Physics, NIKHEF, and University of Amsterdam, NL-1009 DB Amsterdam, The Netherlands
3 University of Michigan, Ann Arbor, MI 48109, USA
4 Laboratoire d'Annecy-le-Vieux de Physique des Particules, LAPP,IN2P3-CNRS, BP 110, F-74941 Annecy-le-Vieux CEDEX, France
5 Institute of Physics, University of Basel, CH-4056 Basel, Switzerland
6 Louisiana State University, Baton Rouge, LA 70803, USA
7 Institute of High Energy Physics, IHEP, 100039 Beijing, China[△]
8 University of Bologna and INFN-Sezione di Bologna, I-40126 Bologna, Italy
9 Tata Institute of Fundamental Research, Mumbai (Bombay) 400 005, India
10 Northeastern University, Boston, MA 02115, USA
11 Institute of Atomic Physics and University of Bucharest, R-76900 Bucharest, Romania
12 Central Research Institute for Physics of the Hungarian Academy of Sciences, H-1525 Budapest 114, Hungary[‡]
13 Massachusetts Institute of Technology, Cambridge, MA 02139, USA
14 Panjab University, Chandigarh 160 014, India
15 KLTE-ATOMKI, H-4010 Debrecen, Hungary[¶]
16 UCD School of Physics, University College Dublin, Belfield, Dublin 4, Ireland
17 INFN Sezione di Firenze and University of Florence, I-50125 Florence, Italy
18 European Laboratory for Particle Physics, CERN, CH-1211 Geneva 23, Switzerland
19 World Laboratory, FBLJA Project, CH-1211 Geneva 23, Switzerland
20 University of Geneva, CH-1211 Geneva 4, Switzerland
21 University of Hamburg, D-22761 Hamburg, Germany
22 Chinese University of Science and Technology, USTC, Hefei, Anhui 230 029, China[△]
23 University of Lausanne, CH-1015 Lausanne, Switzerland
24 Institut de Physique Nucléaire de Lyon, IN2P3-CNRS,Université Claude Bernard, F-69622 Villeurbanne, France
25 Centro de Investigaciones Energéticas, Medioambientales y Tecnológicas, CIEMAT, E-28040 Madrid, Spain[♭]
26 Florida Institute of Technology, Melbourne, FL 32901, USA
27 INFN-Sezione di Milano, I-20133 Milan, Italy
28 Institute of Theoretical and Experimental Physics, ITEP, Moscow, Russia
29 INFN-Sezione di Napoli and University of Naples, I-80125 Naples, Italy
30 Department of Physics, University of Cyprus, Nicosia, Cyprus
31 Radboud University and NIKHEF, NL-6525 ED Nijmegen, The Netherlands
32 California Institute of Technology, Pasadena, CA 91125, USA
33 INFN-Sezione di Perugia and Università Degli Studi di Perugia, I-06100 Perugia, Italy
34 Nuclear Physics Institute, St. Petersburg, Russia
35 Carnegie Mellon University, Pittsburgh, PA 15213, USA
36 INFN-Sezione di Napoli and University of Potenza, I-85100 Potenza, Italy
37 Princeton University, Princeton, NJ 08544, USA
38 University of Californa, Riverside, CA 92521, USA
39 INFN-Sezione di Roma and University of Rome, "La Sapienza", I-00185 Rome, Italy
40 University and INFN, Salerno, I-84100 Salerno, Italy
41 University of California, San Diego, CA 92093, USA
42 Bulgarian Academy of Sciences, Central Lab. of Mechatronics and Instrumentation, BU-1113 Sofia, Bulgaria
43 The Center for High Energy Physics, Kyungpook National University, 702-701 Taegu, Republic of Korea
44 National Central University, Chung-Li, Taiwan, China
45 Department of Physics, National Tsing Hua University, Taiwan, China
46 Purdue University, West Lafayette, IN 47907, USA
47 Paul Scherrer Institut, PSI, CH-5232 Villigen, Switzerland
48 DESY, D-15738 Zeuthen, Germany
49 Eidgenössische Technische Hochschule, ETH Zürich, CH-8093 Zürich, Switzerland
§ Supported by the German Bundesministerium für Bildung, Wissenschaft, Forschung und Technologie.
‡ Supported by the Hungarian OTKA fund under contract numbers T019181, F023259 and T037350.
¶ Also supported by the Hungarian OTKA fund under contract number T026178.
♭ Supported also by the Comisión Interministerial de Ciencia y Tecnología.
♯ Also supported by CONICET and Universidad Nacional de La Plata, CC 67, 1900 La Plata, Argentina.
△ Supported by the National Natural Science Foundation of China.
† Deceased.

References

[1] L3 Collaboration., B. Adeva *et al.*, Nucl. Instr. Meth. **A 289** (1990) 35;
M. Acciarri *et al.*, Nucl. Instr. Meth. **A 351** (1994) 300;
M. Chemarin *et al.*, Nucl. Instr. Meth. **A 349** (1994) 345;
A. Adam *et al.*, Nucl. Instr. Meth. **A 383** (1996) 342;
I. C. Brock *et al.*, Nucl. Instr. Meth. **A 381** (1996) 236.

[2] Review of Particle Physics: W.-M. Yao *et al.*, J. Phys. G: Nucl. Part. Phys. **33** (2006) 1.

[3] L3 Collaboration, M. Acciarri *et al.*, Phys. Lett. **B 501** (2001) 1.

[4] A. V. Anisovich *et al.*, Eur. Phys. J. **A 6** (1999) 247.

[5] T. Barnes, N. Black and P. R. Page Phys. Rev. **D 68** (2003) 054014.

[6] MARK II Collaboration, G. Gidal *et al.*, Phys. Rev. Lett. **59** (1987) 2016.

[7] TPC-2γ Collaboration, H. Aihara *et al.*, Phys. Rev. **D 38** (1988) 1.

[8] JADE Collaboration, P. Hill *et al.*, Z. Phys. **C 42** (1989) 355.

[9] CELLO Collaboration, H.-J. Behrend *et al.*, Z. Phys. **C 42** (1989) 367.

[10] CLEO Collaboration, R. Ahohe *et al.*, Phys. Rev. **D 71** (2005) 072001.

[11] L. D. Landau, *Dokl. Akad. Nauk. USSR* **60** (1948) 207;
C. N. Yang, Phys. Rev. **77** (1950) 242.

[12] G. A. Schuler, F. A. Berends, R. van Gulik, Nucl. Phys. **B 523** (1998) 423.

[13] S. J. Brodsky and G. P. Lepage, Phys. Rev. **D 22** (1980) 2157;
S. J. Brodsky and G. P. Lepage, Phys. Rev. **D 24** (1981) 1808.

[14] L3 Collaboration, P. Achard *et al.*, Phys. Lett. **526** (2002) 269.

[15] R. N. Cahn, Phys. Rev. **D 35** (1987) 3342;
R. N. Cahn, Phys. Rev. **D 37** (1988) 833.

[16] F. L. Linde, *"Charm Production in two-photon Collisions"*, Ph. D. Thesis, Rijksuniversiteit Leiden, (1988).

[17] R. van Gulik, Nucl. Phys. **B 82** (Proc. Suppl.) (2000) 311;
F. A. Berends and R. van Gulik, Comput. Phys. Commun. **144** (2002) 82.

[18] V. M. Budnev *et al.*, Phys. Rep. **C 15** (1975) 181.

[19] R. Brun *et al.*, GEANT 3.15 preprint CERN DD/EE/84-1 (1984), revised 1987.

[20] H. Fesefeldt, RWTH Aachen report PITHA 85/2 (1985).

[21] P. Béné et al., Nucl. Instr. Meth. **A 306** (1991) 150.

[22] D. Haas et al., Nucl. Instr. Meth. **A 420** (1999) 101.

[23] F. E. Close and A. Kirk, Z. Phys. **C 76** (1997) 469.

Q^2 range	ϵ_{TR} (%)	$\epsilon[\mathrm{f_1}(1420)]$ (%)	$\epsilon[\eta\,(1475)]$ (%)	Events	M (MeV)	σ (MeV)
$0 \quad - 0.01$	92 ± 2	0.51 ± 0.03	0.53 ± 0.03	43 ± 9	1464 ± 12	54 ± 10
$0.01 - 0.12$	94 ± 2	0.49 ± 0.05	0.45 ± 0.05	40 ± 9	1462 ± 16	63 ± 20
$0.12 - 0.4$	91 ± 2	0.82 ± 0.10	0.79 ± 0.09	32 ± 7	1426 ± 9	32 ± 8
$0.4 \quad - 0.9$	83 ± 2	1.19 ± 0.15	1.25 ± 0.15	45 ± 9	1453 ± 9	42 ± 9
$0.9 \quad - 7$	67 ± 5	1.92 ± 0.24	1.78 ± 0.22	33 ± 10	1431 ± 19	32 ± 10

Table 1: Results of a Gaussian fit to the peaks of the mass spectra of Figure 3. For each Q^2 range the trigger efficiency, ϵ_{TR}, the overall efficiency of the resonances, ϵ, the number of events, the mass, M, and the width, σ, of the Gaussian peak are presented. All uncertainties are statistical only.

State	Events	M (MeV)	Γ (MeV)	$\Gamma_{\gamma\gamma}\mathrm{BR}(\mathrm{K\bar{K}}\pi)$ (keV)	Λ (MeV)
$\mathrm{f_1}(1420)$	133 ± 23	$1434 \pm 5 \pm 5$	fixed to 55	$3.2 \pm 0.6 \pm 0.7$	$926 \pm 72 \pm 31$
$\eta\,(1475)$	74 ± 16	$1469 \pm 14 \pm 13$	$67 \pm 18 \pm 7$	$0.23 \pm 0.05 \pm 0.05$	fixed to 1470

Table 2: Results of a global fit to the mass spectra of Figure 5. The number of events, the mass, M, and the width, Γ, of the $\mathrm{f_1}(1420)$ and $\eta\,(1475)$ Breit-Wigner functions are given. The two-photon width or the two-photon coupling parameter, $\Gamma_{\gamma\gamma}$, times the branching ratio for the decay to $\mathrm{K\bar{K}}\pi$, $\mathrm{BR}(\mathrm{K\bar{K}}\pi)$, are extracted from the cross sections, estimated with the GaGaRes program from the fitted number of events and the efficiencies of the resonances. The form factor parameter, Λ, is also listed. The first uncertainty is statistical, the second systematic.

	$M(\eta\,(1475))$	$\Gamma(\eta\,(1475))$	$\Gamma_{\gamma\gamma}(\eta\,(1475))\mathrm{BR}(\mathrm{K}\bar{\mathrm{K}}\pi)$	$M(\mathrm{f}_1(1420))$	$\Gamma_{\gamma\gamma}(\mathrm{f}_1(1420))\mathrm{BR}(\mathrm{K}\bar{\mathrm{K}}\pi)$	$\Lambda(\mathrm{f}_1(1420))$
$M(\eta\,(1475))$	1					
$\Gamma(\eta\,(1475))$	-0.20	1				
$\Gamma_{\gamma\gamma}(\eta\,(1475))\mathrm{BR}(\mathrm{K}\bar{\mathrm{K}}\pi)$	0.09	-0.42	1			
$M(\mathrm{f}_1(1420))$	-0.06	-0.11	-0.02	1		
$\Gamma_{\gamma\gamma}(\mathrm{f}_1(1420))\mathrm{BR}(\mathrm{K}\bar{\mathrm{K}}\pi)$	0.38	-0.21	0.11	0.08	1	
$\Lambda(\mathrm{f}_1(1420))$	-0.28	0.20	-0.20	-0.04	-0.69	1

Table 3: Correlation coefficients for the free parameters of the global fit shown in Figure 5.

Source	$\Gamma(\eta\,(1475))$	$\Gamma_{\gamma\gamma}(\eta\,(1475))\mathrm{BR}(\mathrm{K}\bar{\mathrm{K}}\pi)$	$\Gamma_{\gamma\gamma}(\mathrm{f}_1(1420))\mathrm{BR}(\mathrm{K}\bar{\mathrm{K}}\pi)$	$\Lambda_1(\mathrm{f}_1(1420))$
K^0_S mass	2.1	8.5	3.0	2.0
K^0_S decay vertex	9.4	4.1	4.8	1.8
$\mathrm{d}E/\mathrm{d}x$ selection	4.3	19.5	15.6	2.7
$\eta\,(1475)$ form factor	2.3	1.2	2.6	–
$\mathrm{f}_1(1420)$ width	2.0	1.3	2.7	0.2
Efficiency	0.3	5.4	13.8	0.1

Table 4: Systematic uncertainties on the fit parameters, in percent. The systematic uncertainties on the masses are below 1%

State	M (MeV)	Number of events
$\mathrm{K}^\pm\pi^\mp$	879 ± 9	62 ± 15
$\mathrm{K}^0_\mathrm{S}\pi^\pm$	880 ± 6	67 ± 15

Table 5: Results of the fit to the mass spectra of Figure 7. The mass, M, and the number of events in the peak are given with their statistical uncertainties.

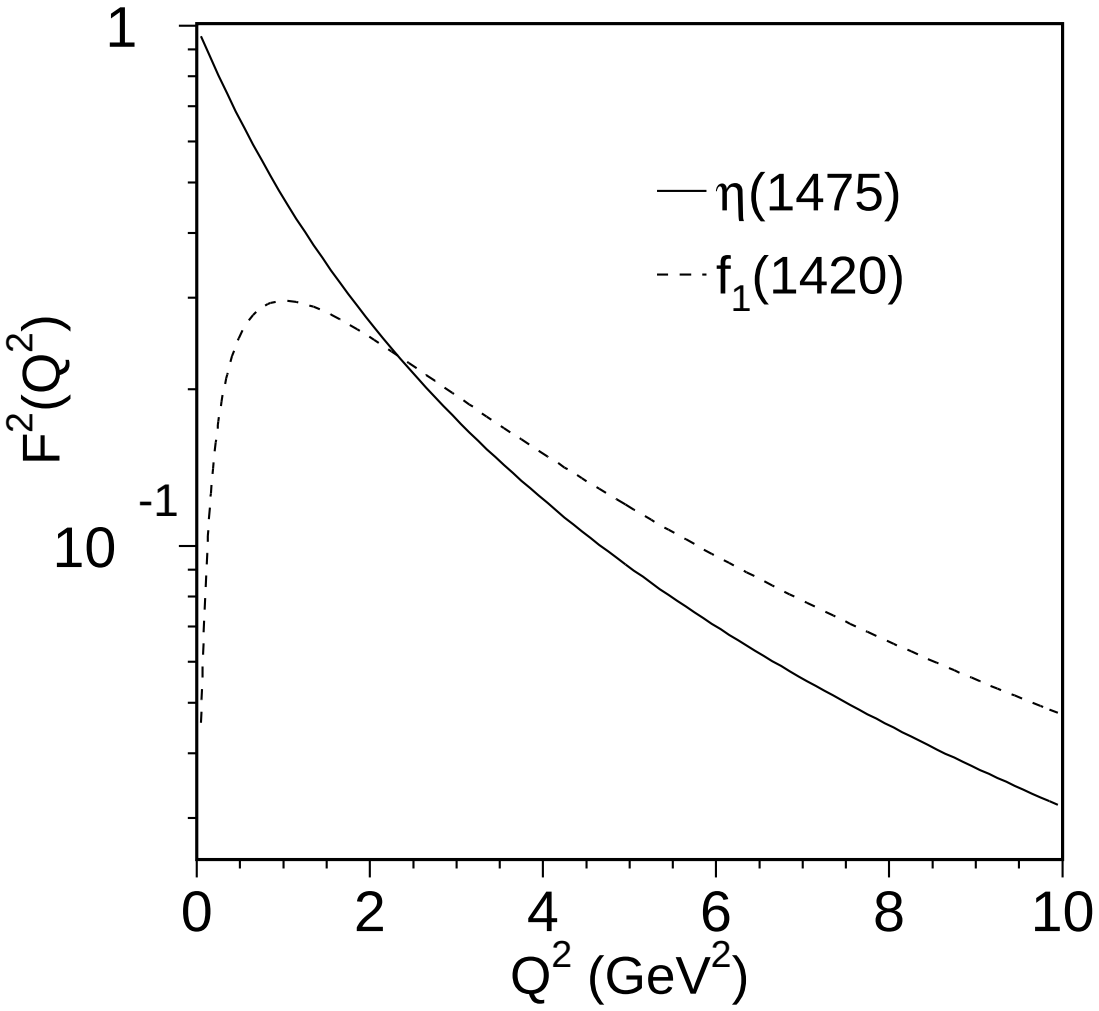

Figure 1: Dependence on Q^2 of the square of the form factors of the $\eta\,(1475)$ (solid line) and $f_1(1420)$ (dashed line) mesons. The form factor parameters of formulae (2) and (3) are chosen as $\Lambda_0 = 1470$ MeV and $\Lambda_1 = 1420$ MeV, respectively.

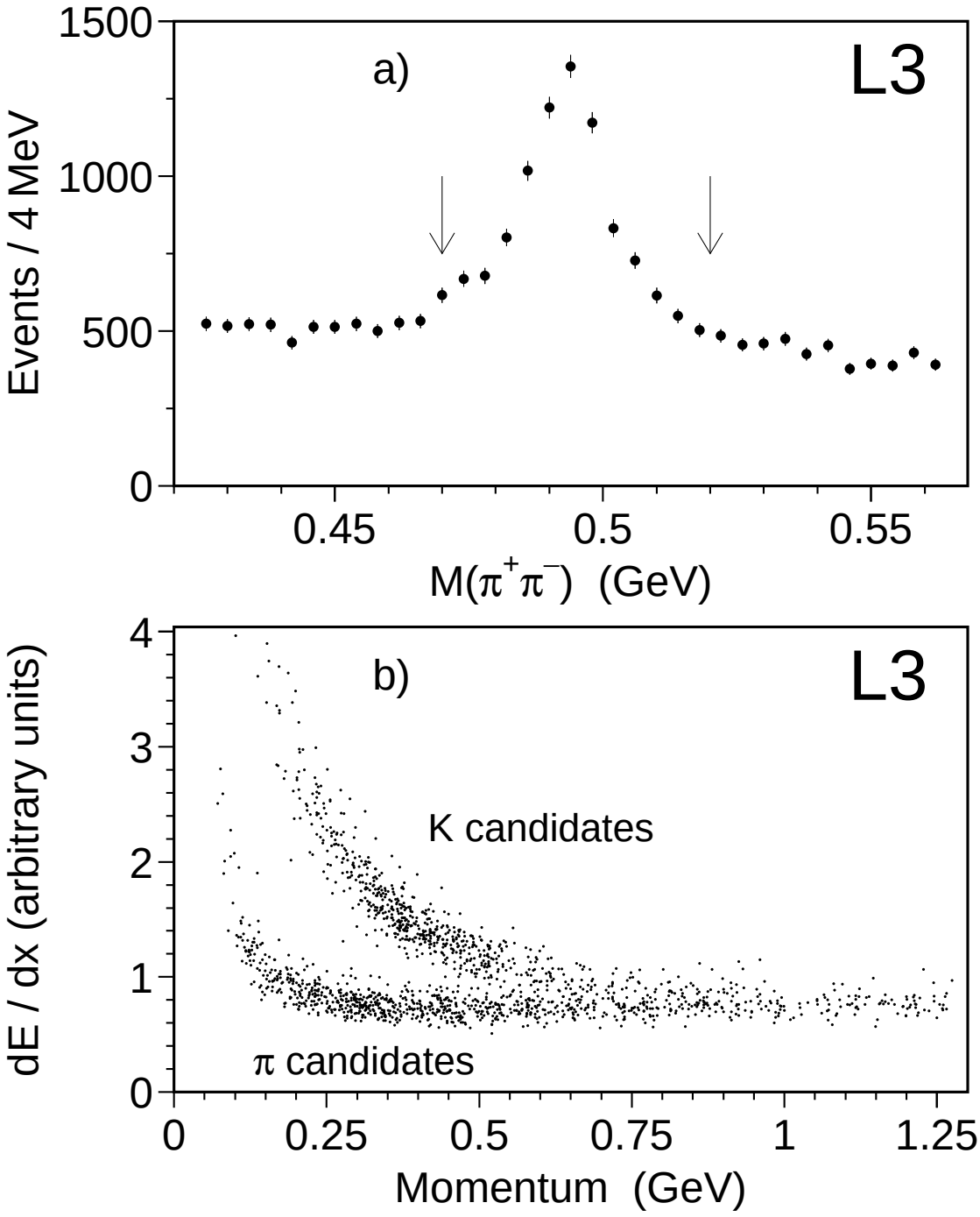

Figure 2: a) Spectrum of the $\pi^+\pi^-$ mass before any other selection cut. The arrows indicate the K^0_S candidate window. b) The dE/dx distribution for charged particles at the e^+e^- interaction vertex.

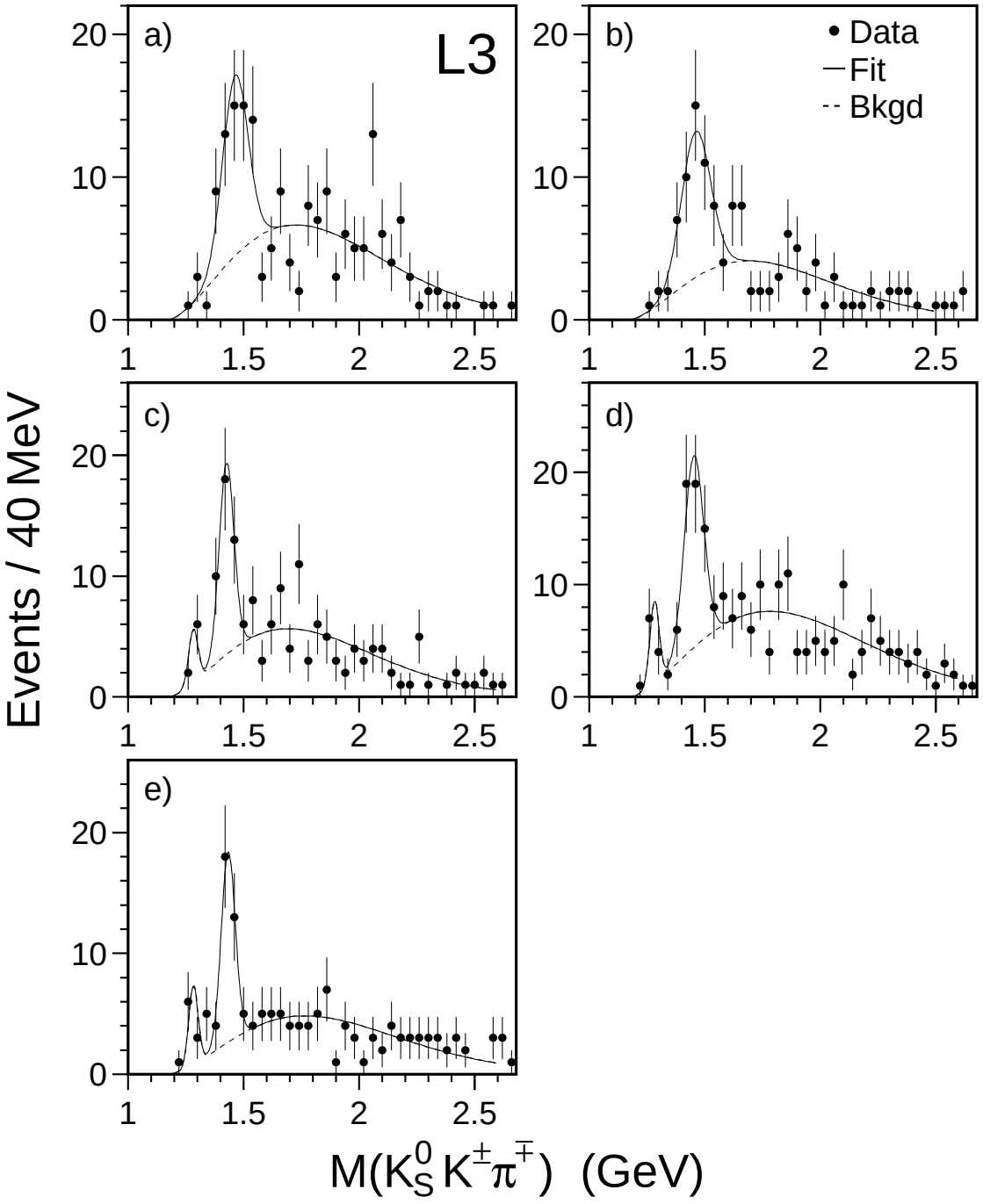

Figure 3: The $K^0_S K^{\pm}\pi^{\mp}$ effective mass spectra for five Q^2 bins: a) $0 - 0.01$ GeV^2; b) $0.01 - 0.12$ GeV^2; c) $0.12{-}0.4$ GeV^2; d) $0.4{-}0.9$ GeV^2; e) $0.9{-}7$ GeV^2. Fits of a Gaussian function over a Q^2-dependent background are superimposed on the data. For spectra with $Q^2 > 0.12$ GeV^2, an additional Gaussian function, representing the $f_1(1285)$, is added with fixed mass and width: $M = 1282$ MeV and $\sigma = 20$ MeV.

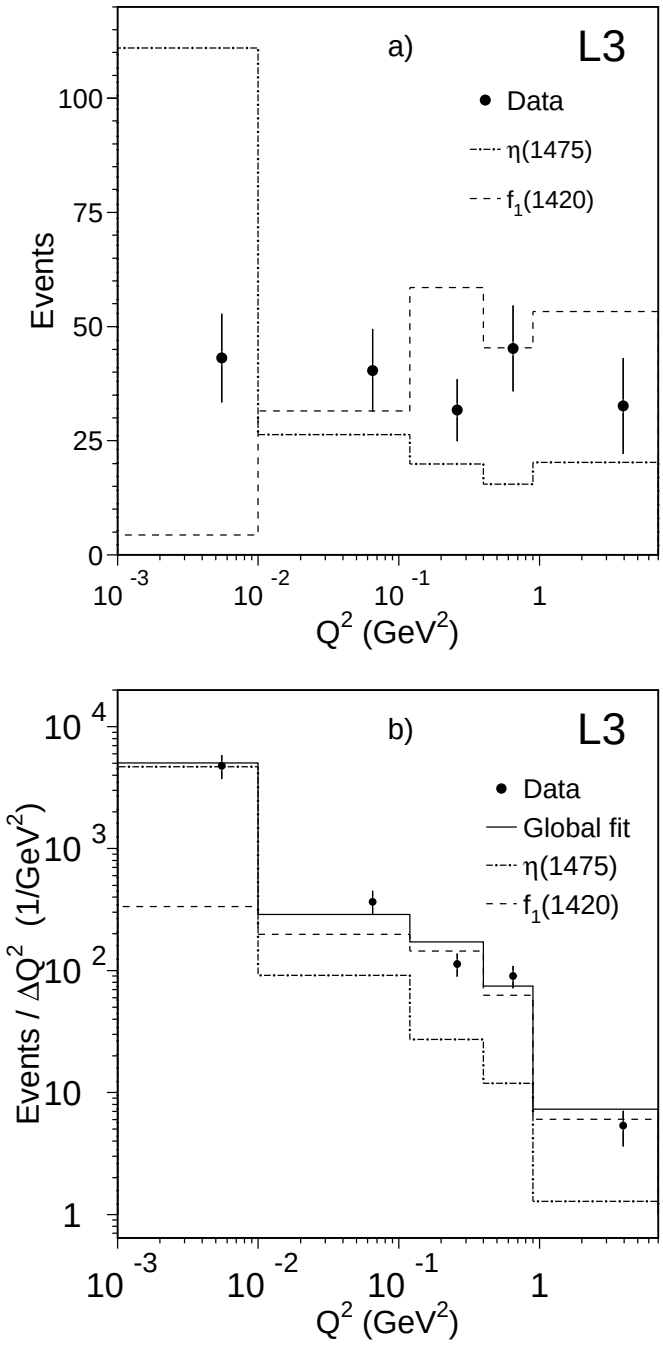

Figure 4: a) Number of events obtained by the Gaussian fit presented in Table 1 and Figure 3 compared to Monte Carlo predictions in presence of a single resonance, either the $\eta\,(1475)$ (dotted-dashed line) or the $\mathrm{f}_1(1420)$ (dashed line). b) Number of events per ΔQ^2 range observed in data, together the results of a global fit (solid line) including two contributions: $\mathrm{f}_1(1420)$ (dashed line) and $\eta\,(1475)$ (dotted-dashed line). In both figures the uncertainties are statistical only.

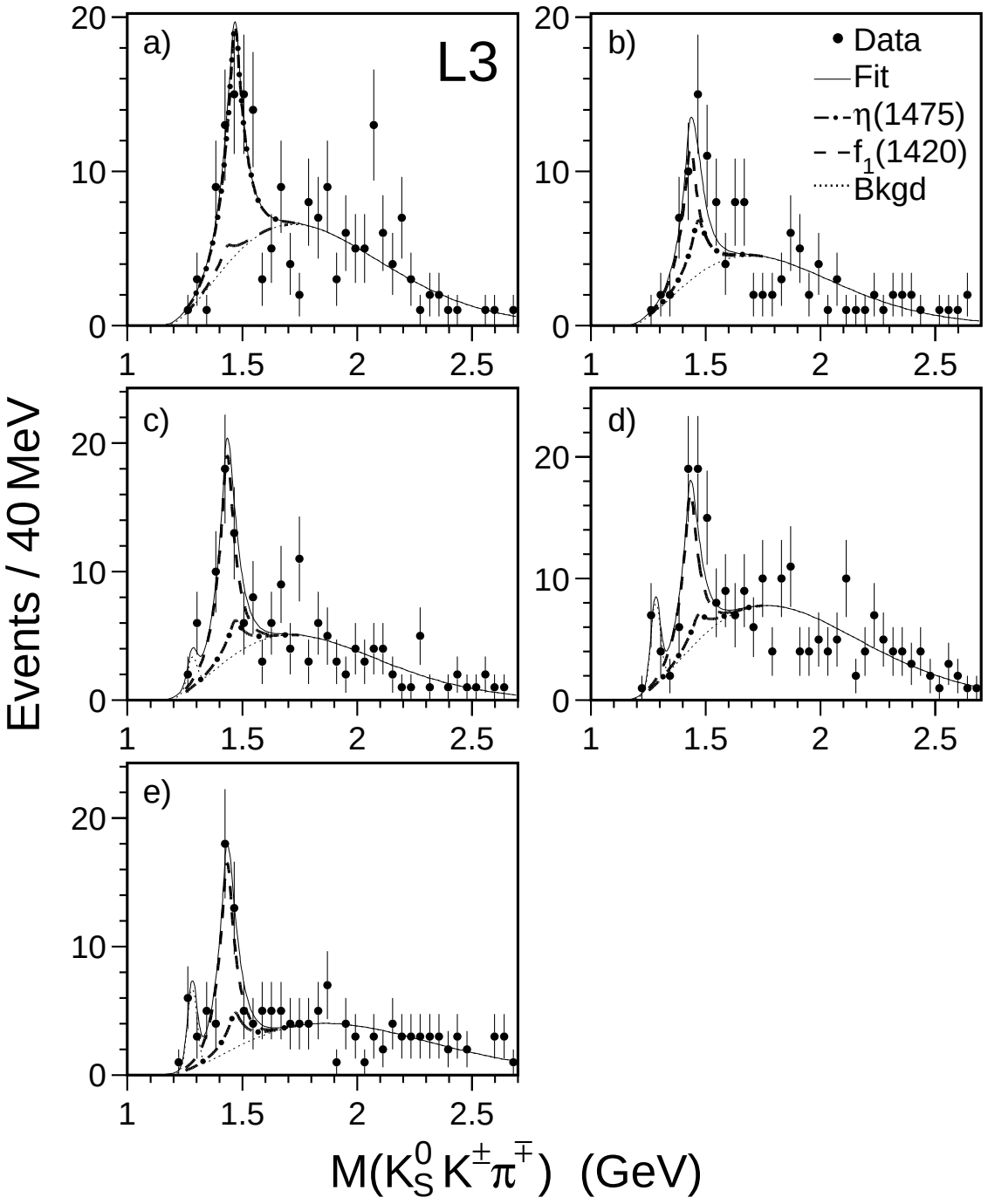

Figure 5: The $K^0_S\,K^{\pm}\pi^{\mp}$ effective mass spectra for the five Q^2 ranges: a) $0-0.01$ GeV^2, b) $0.01-0.12$ GeV^2, c) $0.12-0.4$ GeV^2, d) $0.4-0.9$ GeV^2, e) $0.9-7$ GeV^2. Results of a global fit of two resonances over a Q^2-dependent background are also shown. For the spectra with $Q^2 > 0.12$ GeV^2, an additional Gaussian function, representing the $f_1(1285)$, is added with fixed mass and width: $M = 1282$ MeV and $\sigma = 20$ MeV.

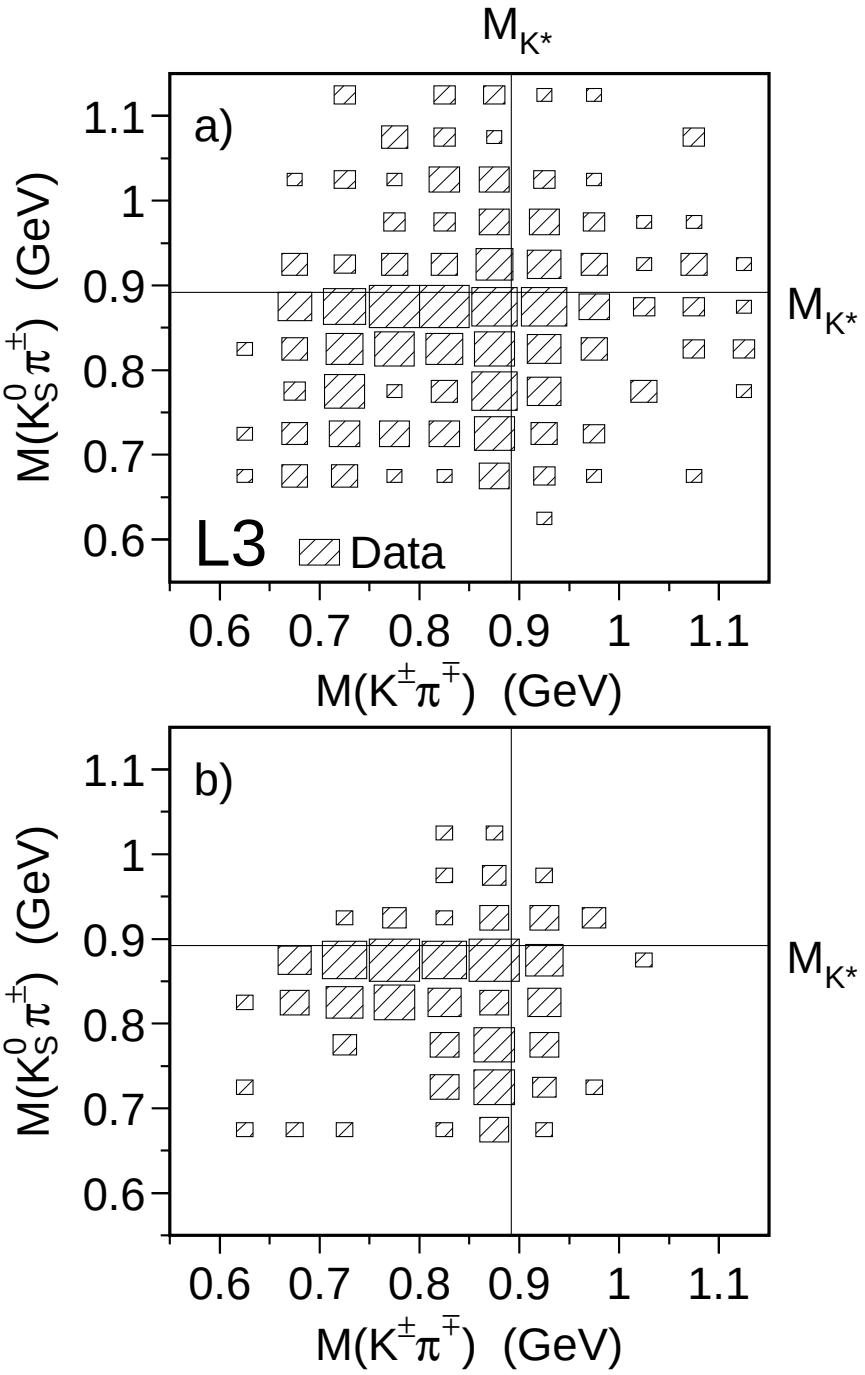

Figure 6: Two-dimensional mass distributions used for the study of the $f_1(1420) \to K^*(892)K$ decay mode for $Q^2 > 0.4$ GeV^2. a) Data for the entire $K^0_S K^\pm\pi^\mp$ mass range and b) data in the resonance region: $1320 \leq M(K^0_S K^\pm\pi^\mp) \leq 1570$ MeV. The solid lines indicate the $K^*(892)$ mass, $M_{K^*} = 892$ MeV.

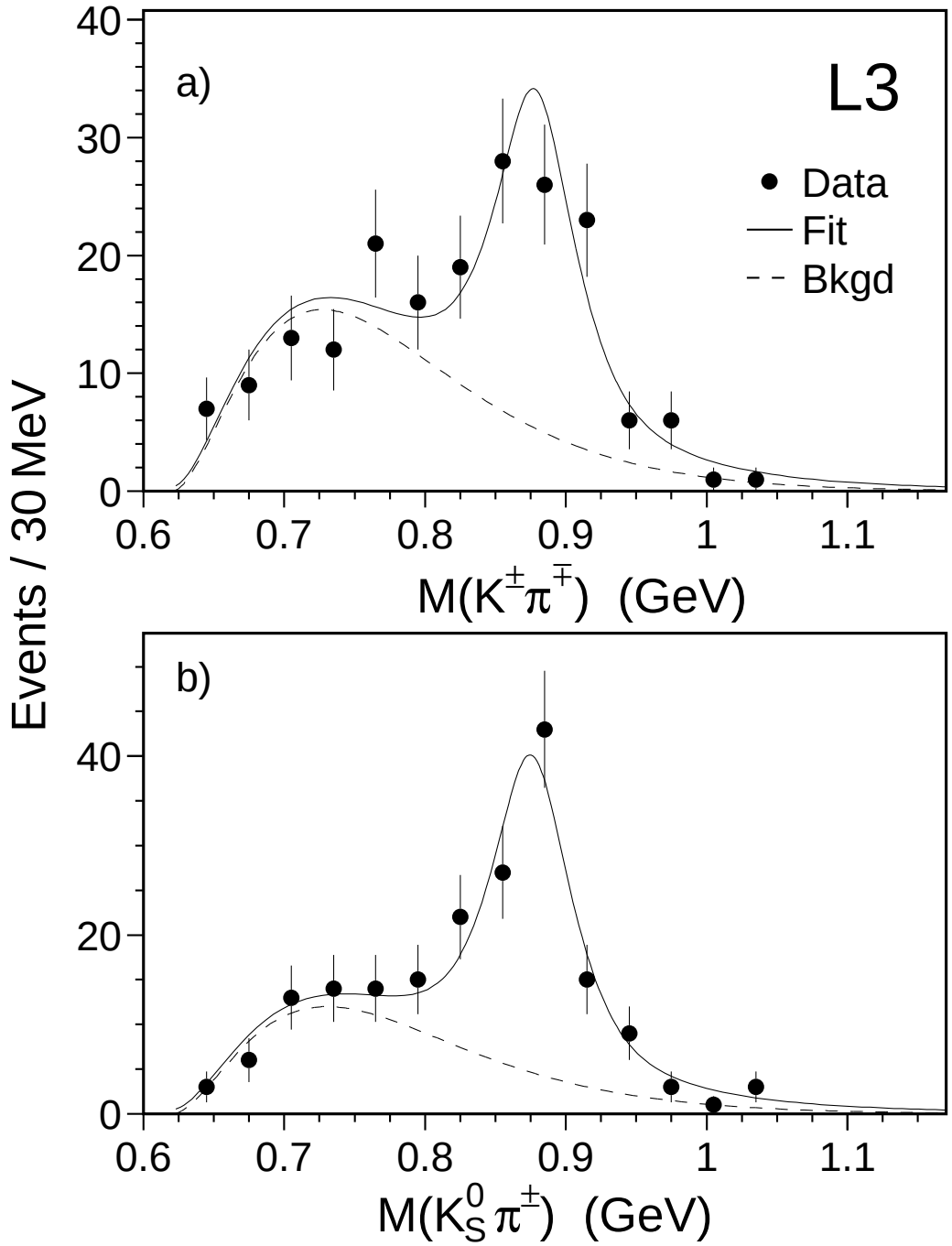

Figure 7: Mass spectra for a) $\mathrm{K}^{\pm}\pi^{\mp}$ and b) $\mathrm{K}^0_{\mathrm{S}}\pi^{\pm}$ combinations for $1320 \leq M(\mathrm{K}^0_{\mathrm{S}}\,\mathrm{K}^{\pm}\pi^{\mp}) \leq 1570$ MeV and $Q^2 > 0.4$ GeV^2. Fits of a resonance over a background are superimposed on the data.